Non-orthogonal Multiple Access Enabled Two-layer GEO/LEO Satellite Network

Ruixing Ge†, Jian Cheng†*, Kang An‡, Gan Zheng♭

†. College of Communication Engineering, Army Engineering University of PLA, Nanjing, China

‡. The Sixty-third Research Institute, National University of Defense Technology, Nanjing, China

♭. Wolfson School of Mechanical, Electrical, and Manufacturing Engineering, Loughborough University, Loughborough, U.K.

(Emails: geruixing1993@sina.com, chjatice@163.com, ankang89@nudt.edu.cn, g.zheng@lboro.ac.uk)

*Corresponding Author: Jian Cheng

***Abstract*—The construction and operation of multi-layer heterogeneous satellite network (MLSNs) have gain significant attention due to its multiple capabilities and functionalities. This paper investigates the capacity performance of a two-layer geostationary earth orbit (GEO)/ low earth orbit (LEO) satellite network, where the non-orthogonal multiple access (NOMA) scheme is incorporated in a frequency coexistence scenario to improve the spectral efficiency. Specifically, a two-layer GEO/LEO satellite network framework is established by considering the dynamic properties and transmission characteristics of different satellites under practical environment. Then, the theoretical expression of achievable ergodic capacity is derived in terms of Meijer-G functions to evaluate the system performance effectively. Finally, simulation results are provided to validate the theoretical results, show the superiority of the employed NOMA scheme and analysis the impact of various system parameters on capacity performance of the considered network.**

***Index Terms*—Two-layer satellite network, non-orthogonal multiple access, ergodic capacity**

I. Introduction

Multi-layer satellite networks (MLSNs) have been proposed as a practical architecture of next generation satellite networks which can realize functionally integration of different orbital satellites [1]. However, in addition to the frequency coexistence between satellite and terrestrial systems, MLSNs also face in-line interference from geostationary earth orbit (GEO) and non-geostationary (NGEO) satellites due to the heterogeneous framework [2], [3]. Currently, several methods have been adopted to solve the frequency interference coordination problem problem in different scenarios, including power control technique in hybrid satellite-terrestrial networks to realize spectrum sharing [4], [5] and progressive pitch technique in LEO satellite constellations [6] to mitigate the interference to GEO satellites.

Recently, non-orthogonal multiple access (NOMA) has received considerable interest in satellite communication networks for its superior spectral efficiency. Both theoretical analysis and numerical simulations have validated the effectiveness and superiority of the NOMA scheme in various scenarios. Particularly, key performance merits are analyzed in NOMA-based satellite networks in both GEO and LEO satellite networks [7], [8]. Considering the interference from the terrestrial communication network, ergodic capacity and outage probability performances in NOMA-based cognitive hybrid satellite-terrestrial networks were further analyzed in [9] and [10], respectively. For uplink transmission cases, the system performances were investigated considering the impact of random deployment of the terrestrial users [11] and detecting methods at the receiver [12]. In addition, power allocation schemes were investigated in [13] and [14] to enhance the fairness of multibeam satellite networks employing the NOMA scheme. A joint user pairing, precoding, and power allocation scheme was proposed in [15] to maximize the system capacity in integrated terrestrial-satellite networks, and a multiuser pairing method combined with beamforming scheme was further studied in [16]. However, it can be observed that these works mainly focus on single satellite networks without considering the application of NOMA in MLSNs.

Noticing that the heterogeneity of channel condition between GEO and LEO satellite can be exploited to employ NOMA scheme in MLSNs under the aforementioned frequency coexistence scenario, this paper investigate the performance of a two-layer GEO/LEO satellite network enabling the NOMA scheme. Specifically, the system model is analyzed considering the dynamic properties and transmission characteristics of different satellite nodes. The achievable ergodic capacity expression is derived in terms of Meijer-G functions and approximated using Gaussian-Chebyshev Quadrature (GCQ) to provide an efficient approach to evaluate the system performance. Simulation results are provided to confirm the validity of the theoretical formulas, the superiority of employing the NOMA scheme, and the impacts of various parameters on the performance of the considered network.

II. System model

As illustrated in Fig.1, we consider a two-layer satellite network enabling the NOMA scheme where a ground user (U) transmits signal to GEO satellite (S_{GEO}) and LEO satellite (S_{LEO}) simultaneously occupying same frequency resource block. Node U, S_{LEO} and S_{GEO} are all equipped with one single antenna.

Following the principle of NOMA, the ground user U broadcasts a superposed signal to S_{LEO} and S_{GEO}. Using

ISBN: 978-9-0827-9706-0

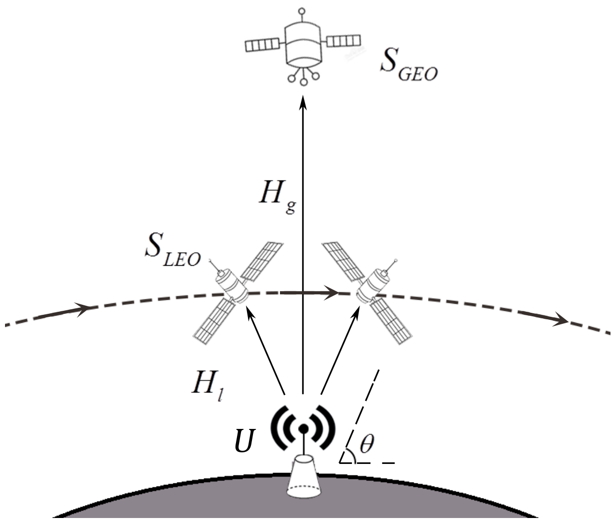

Fig. 1. System model of a two-layer satellite network

g and l to represent S_{GEO} and S_{LEO}, the observation at the satellite nodes can be expressed as

$$y_k = \sqrt{H_k}(\sqrt{\alpha P_s}x_l + \sqrt{(1-\alpha)P_s}x_g) + n_k, \quad k \in \{g, l\}, \tag{1}$$

where P_s denotes the transmit power at node U, α denotes the power allocation coefficient which is the fraction of transmit power allocated to S_{LEO}, x_k is the transmit signal to the satellite nodes with $\mathrm{E}[|x_k|^2] = 1$, H_k denotes the channel coefficient between the satellite nodes and U, n_k denotes the additive white Gaussian noise (AWGN) at the satellite nodes with $\mathrm{E}[|n_k|^2] = \sigma_k^2$.

The channel coefficient H_k consist of free space loss, antenna gain and channel fading factor

$$H_k = L_k G_u G_k(\varphi_k)|h_k|^2, \tag{2}$$

where G_u denotes the antenna gain at node U, $G_k(\varphi_k)$ denotes the antenna gain at the satellite nodes which is a function of angle φ_k (the angle between ground user and the beam center with respect to the satellite). In this paper, S_{LEO} is supposed to operate under the staring beam mode so $G_k(\varphi_k)$ can be viewed as constant G_k.

L_k denotes the free space loss of the transmission link which can be calculated as $L_k = (c/4\pi f d_k)^2$, where c, f and d_k denote the light speed, the carrier frequency and the transmission distance, respectively.

For S_{GEO}, L_g is a constant due to the geostationary orbit. For S_{LEO}, L_l is time-varying due to the relative movement between S_{LEO} and U. The varying distance d_l can be expressed as a function of LEO elevation angle θ with respect to U.

$$d_{tl}(\theta) = \sqrt{R_e^2 \sin^2\theta + h_l^2 + 2h_l R_e} - R_e \sin\theta, \theta \in [0, \frac{\pi}{2}], \tag{3}$$

where R_e denotes the earth radius and h_l denotes the altitude of S_{LEO}.

It is worth mentioning that the NOMA scheme is employed under a frequency coexistence scenario when the in-line interference arises. Thus, elevation angle θ is limited in a certain range from $\theta_{\max}$ to $\theta_{\min}$. The probability density function (PDF) of elevation angle θ can be expressed by (4) with a prescribed maximum elevation angle and minimum elevation angle [15]

$$f_\theta(x) = \frac{G(x)\sin(\phi(x))}{\sqrt{\cos^2(\phi(\theta_{\max})) - \cos^2(\phi(x))}\cos^{-1}\left(\frac{\cos(\phi(\theta_{\min}))}{\cos(\phi(\theta_{\max}))}\right)}, \tag{4}$$

where $\phi(\theta) = \cos^{-1}(a \cdot \cos\theta) – \theta$, $G(\theta) = \dfrac{1 + a^2 - 2a\cos(\phi(\theta))}{1 - a\cos(\phi(\theta))}$ and $a = \dfrac{R_e}{R_e + h_l}$.

$|h_k|^2$ denotes the fading channel factor between U and each satellite node which undergoes shadowed-Rician fading distribution [18]. The PDF of $|h_k|^2$ is given by

$$f_{|h_k|^2}(x) = \alpha_k e^{-\beta_k x} {}_1F_1(m_k; 1; \delta_k x), \tag{5}$$

where $\alpha_k = (2b_k m_k/(2b_k m_k + \Omega_k))^{m_k}/2b_k$, $\beta_k = 1/2b_k$, $\delta_k = \Omega_k/2b_k/(2b_k m_k + \Omega_k)$, Ω_k and $2b_k$ are average power of line-of-sight and multipath components, respectively. m_k is the Nakagami-*m* parameter. ${}_1F_1(\cdot)$ is the confluent hypergeometric function [19, eq. (9.100)].

Here we assume that the satellite-terrestrial channel fading factors $|h_g|^2$ and $|h_l|^2$ are independent and identically distributed (i.i.d.). This is due to the fact that the shadowed-Rician fading model of the satellite-terrestrial channel depends on both the propagation environment and elevation angle respect to the satellite [18].

By employing the NOMA scheme in the considered network, S_{GEO} with higher altitude and worse channel condition is allocated with more power and decodes its information directly. S_{LEO} with lower altitude and better channel condition is allocated with less power and decodes its information by carrying out successive interference cancellation (SIC).

Specifically, S_{LEO} first decodes the information of S_{GEO} and then decodes its own information after subtracting the former information. The SINRs of S_{GEO} and S_{LEO} satellites are given by

$$\gamma_g = \frac{(1-\alpha)P_s H_g}{\alpha P_s H_g + \sigma_g^2} = \frac{(1-\alpha)\bar{\gamma}_g H_g}{\alpha \bar{\gamma}_g H_g + 1}, \quad \gamma_l = \frac{\alpha P_s H_l}{\sigma_l^2} = \alpha \bar{\gamma}_l H_l, \tag{6}$$

where $\bar{\gamma}_g = P_s/\sigma_g^2$ and $\bar{\gamma}_l = P_s/\sigma_l^2$.

Furthermore, in order to ensure the NOMA scheme can achieve a larger transmission rate than traditional orthogonal multiple access (OMA) scheme, the power allocation coefficient α is expressed as [20]

$$\alpha = \frac{\varepsilon_g}{\sqrt{1 + \bar{\gamma}_g H_g} + 1} + \frac{\varepsilon_l}{\sqrt{1 + \bar{\gamma}_l H_l} + 1}, \tag{7}$$

where $0 \le \varepsilon_l, \varepsilon_g \le 1$ and $\varepsilon_l + \varepsilon_g = 1$.

It can be observed from (7) that the maximum sum rate can be obtained when $\varepsilon_g = 1, \varepsilon_1 = 0$. By substituting (7) into (6) along with some simplification, $R_{\rm sum}^{\max}$ can be expressed as

$$\begin{aligned} R_{\rm sum}^{\max} &= \log_2(1+\gamma_l)+\log_2(1+\gamma_g) \\ &= \log_2(1+\alpha\bar{\gamma}_l H_l)+\log_2\left(\frac{\bar{\gamma}_g H_g+1}{\alpha\bar{\gamma}_g H_g+1}\right) \\ &= \log_2\left(\sqrt{1+\bar{\gamma}_g H_g}\right)+\log_2\left(1+\frac{\bar{\gamma}_l H_l}{\sqrt{1+\bar{\gamma}_g H_g}+1}\right). \end{aligned} \tag{8}$$

III. Ergodic Capacity Analysis

From the analysis above, the system ergodic capacity with maximize transmission rate can be express as

$$\begin{aligned} C_{\rm erg}^{\max} &= \mathrm{E}\left[\log_2\left(\sqrt{1+\bar{\gamma}_g H_g}\right)\right]+\mathrm{E}\left[\log_2\left(1+\frac{\bar{\gamma}_l H_l}{\sqrt{1+\bar{\gamma}_g H_g}+1}\right)\right] \\ &= \underbrace{\mathrm{E}\left[\log_2\left(1+\bar{\gamma}_l H_l+\sqrt{1+\bar{\gamma}_g H_g}\right)\right]}_{C_1} \\ &\quad -\underbrace{\mathrm{E}\left[\log_2\left(1+\sqrt{1+\bar{\gamma}_g H_g}\right)\right]}_{C_2}+\underbrace{\mathrm{E}\left[\log_2\left(\sqrt{1+\bar{\gamma}_g H_g}\right)\right]}_{C_3}. \end{aligned} \tag{9}$$

To further evaluate the system ergodic capacity, we divide (9) into three parts: C_1, C_2, and C_3, the derivations are as follows.

A. Computation of C_1

For C_1, we first derive its approximated expression with the help of Taylor series

$$C_1 \approx \log_2(e)\left[\ln(1+\mathrm{E}[\Theta])-\frac{\mathrm{E}[\Theta^2]-\mathrm{E}^2[\Theta]}{2(1+\mathrm{E}[\Theta])^2}\right], \tag{10}$$

where $\Theta=\bar{\gamma}_l H_l+\sqrt{1+\bar{\gamma}_g H_g}$. Since $|h_g|^2$, $|h_l|^2$ and θ are independent of each other, $\mathrm{E}[\Theta]$ and $\mathrm{E}[\Theta^2]$ can be expressed as

$$\mathrm{E}[\Theta]=\mathrm{E}[\bar{\gamma}_l H_l]+\mathrm{E}[\sqrt{1+\bar{\gamma}_g H_g}], \tag{11}$$

$$\mathrm{E}[\Theta^2]=\mathrm{E}[\bar{\gamma}_l^2 H_l^2]+2\mathrm{E}[\bar{\gamma}_l H_l]\mathrm{E}[\sqrt{1+\bar{\gamma}_g H_g}]+\mathrm{E}[1+\bar{\gamma}_g H_g]. \tag{12}$$

With the help of (2) and (6), $\mathrm{E}[\bar{\gamma}_l H_l]$ can be expressed as

$$\mathrm{E}[\bar{\gamma}_l H_l]=\bar{\gamma}_l\int_{\theta_{\min}}^{\theta_{\max}}\xi_l(x)f_\theta(x)\int_0^\infty y f_{|h_l|^2}(y)\,dy\,dx, \tag{13}$$

where $\xi_l(x)=L_l(x)G_uG_l$.

With the help of [19, eq. (9.34.8)] and [19, eq. (7.813.1)], (13) can be expressed in terms of Meijer-G function [19, eq. (9.301)]

$$\begin{aligned} \mathrm{E}[\bar{\gamma}_l H_l] &= \frac{\bar{\gamma}_l\alpha_l}{\beta_l^2\Gamma(m_l)}\,G_{2,2}^{1,2}\left[\frac{-\delta_l}{\beta_l}\middle|\begin{matrix}-1,1-m_l\\0,0\end{matrix}\right] \\ &\quad\times\int_{\theta_{\min}}^{\theta_{\max}}\xi_l(x)f_\theta(x)\,dx, \end{aligned} \tag{14}$$

where $\Gamma(\cdot)$ is the complete gamma function [19, eq. (8.310.1)].

This integral can be further approximated using GCQ [21]

$$\begin{aligned} \mathrm{E}[\bar{\gamma}_l H_l] &\approx \sum_{i=1}^{N}\frac{\omega_i\kappa\bar{\gamma}_l\alpha_l}{\beta_l^2\Gamma(m_l)}\xi_l(\kappa x_i+\kappa^*)f_\theta(\kappa x_i+\kappa^*) \\ &\quad\times G_{2,2}^{1,2}\left[\frac{-\delta_l}{\beta_l}\middle|\begin{matrix}-1,1-m_l\\0,0\end{matrix}\right], \end{aligned} \tag{15}$$

where $\kappa=(\theta_{\max}-\theta_{\min})/2$, $\kappa^*=(\theta_{\max}+\theta_{\min})/2$, τ_i is the i-th zero of Legendre polynomials and ω_i is the Gaussian weight factor shown in [21, tab. (25.4)].

Following the same step, $\mathrm{E}[\bar{\gamma}_l^2 H_l^2]$ can also be expressed as

$$\begin{aligned} \mathrm{E}[\bar{\gamma}_l^2 H_l^2] &\approx \sum_{i=1}^{N}\frac{\omega_i\kappa\bar{\gamma}_l^2\alpha_l}{\beta_l^3\Gamma(m_l)}\xi_l^2(\kappa x_i+\kappa^*)f_\theta(\kappa x_i+\kappa^*) \\ &\quad\times G_{2,2}^{1,2}\left[\frac{-\delta_l}{\beta_l}\middle|\begin{matrix}-2,1-m_l\\0,0\end{matrix}\right]. \end{aligned} \tag{16}$$

Noticing that H_g only has one variable $|h_g|^2$, $\mathrm{E}[1+\bar{\gamma}_g H_g]$ can be written as

$$\mathrm{E}[1+\bar{\gamma}_g H_g]=1+\frac{\bar{\gamma}_g\xi_g\alpha_g}{\beta_g^2\Gamma(m_g)}G_{2,2}^{1,2}\left[\frac{-\delta_g}{\beta_g}\middle|\begin{matrix}-1,1-m_g\\0,0\end{matrix}\right]. \tag{17}$$

To compute $\mathrm{E}[\sqrt{1+\bar{\gamma}_g H_g}]$, we first express $\sqrt{1+\bar{\gamma}_g H_g}$ in terms of Meijer-G function with the help of [22, eq. (10)]

$$\mathrm{E}\left[\sqrt{1+\bar{\gamma}_g H_g}\right]=\mathrm{E}\left[\frac{1}{\Gamma(-0.5)}G_{1,1}^{1,1}\left[\bar{\gamma}_g H_{sg}\middle|\begin{matrix}1.5\\0\end{matrix}\right]\right]. \tag{18}$$

With the help of [19, eq. (9.34.8)] and [23, eq. (2,6,2)], (18) can be computed as

$$\begin{aligned} &\mathrm{E}\left[\sqrt{1+\bar{\gamma}_g H_g}\right] \\ &=\alpha_g(\Gamma(-0.5)\Gamma(m_g)\beta_g)^{-1} \\ &\quad\times G_{1,[1:1],0,[1:2]}^{1,1,1,1,1}\left[\begin{matrix}\frac{\bar{\gamma}_g\xi_g}{\beta_g}\\ \frac{-\delta_g}{\beta_g}\end{matrix}\middle|\begin{matrix}(1,1)\\1.5;1-m_g\\---\\0;(0,0)\end{matrix}\right]. \end{aligned} \tag{19}$$

where $\xi_g=L_gG_uG_g$, $G_{1,[1:1],0,[1,2]}^{1,1,1,1,1}[\cdot|\cdot]$ is the generalized Meijer-G functions with two variables.

Then, the closed-from expressions of $\mathrm{E}[\Theta]$ and $\mathrm{E}[\Theta^2]$ can be derived by substituting (15), (16), (17) and (19) into (11) and (12). Moreover, C_1 can be computed by substituting $\mathrm{E}[\Theta]$ and $\mathrm{E}[\Theta^2]$ into (10).

B. Computation of C_2 and C_3

To compute C_2, the approximated expression can also be expressed as

$$P_2 \approx \log_2(e)[\ln(1+\mathrm{E}[\Xi])-\frac{\mathrm{E}[\Xi^2]-\mathrm{E}^2[\Xi]}{2(1+\mathrm{E}[\Xi])^2}], \tag{20}$$

where $\Xi=\sqrt{1+\bar{\gamma}_g H_g}$.

From the analyses above, $\mathrm{E}[\Xi]$ and $\mathrm{E}[\Xi^2]$ have been expressed in (17) and (19). Hence C_2 can be computed by substituting (17) and (19) into (20).

For C_3, we first express $\mathrm{E}\left[\log_2\left(\sqrt{1+\bar{\gamma}_g H_g}\right)\right]$ in terms of Meijer-G function with the help of [22, eq. (11)]

$$\mathrm{E}\left[\log_2\left(\sqrt{1+\bar{\gamma}_g H_g}\right)\right]=\frac{1}{2\ln 2}\mathrm{E}\left[G_{2,2}^{1,2}\left[\bar{\gamma}_g H_g\middle|\begin{matrix}1,1\\1,0\end{matrix}\right]\right]. \tag{21}$$

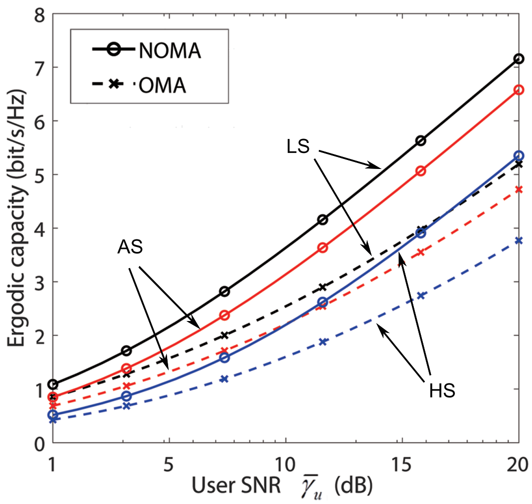

Fig. 2. Ergodic capacity versus user SNR $\overline{\gamma}_u$

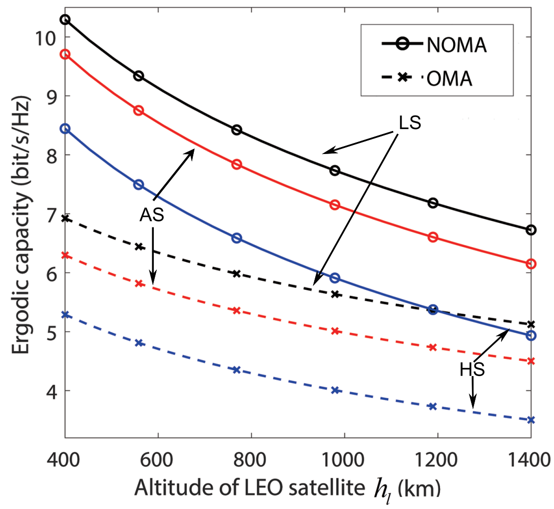

Fig. 3. Ergodic capacity versus LEO satellite altitude

Utilizing [19, eq. (9.34.8)] and [23, eq. (2,6,2)], C_3 can be computed as

$$\begin{aligned}
&\mathrm{E}\left[\log_2\left(\sqrt{1+\bar{\gamma}_g H_g}\right)\right] \\
&= \alpha_g\left(2\ln 2\Gamma(m_g)\beta_g\right)^{-1} \\
&\quad \times G^{1,2,1,1,1}_{1,[2:1],0,[2:2]}\left[\begin{array}{c|c} \dfrac{\bar{\gamma}_g\xi_g}{\beta_g} & \begin{array}{c}(1,1)\\ 1,1;1-m_g\end{array} \\ \dfrac{-\delta_g}{\beta_g} & \begin{array}{c}---\\ (1,0);(0,0)\end{array}\end{array}\right].
\end{aligned} \tag{22}$$

Finally, $C^{\max}_{\text{erg}}$ of the system can be expressed and approximated by substituting C_1, C_2 and C_3 into (9).

IV. Simulation Results

This section provides numerical results to validate the derived theoretical analysis and investigates the impact of various system parameters on system performance. In the simulations, the network is operating under the central frequency of 14GHz in Ku band, the signal bandwidth B is 10MHz, the maximum elevation angle of LEO satellite is set as $\theta_{\max} = 90^{\text{o}}$, the beam gain $G_u = 20\text{dBi}$, $G_g = 40\text{dBi}$ and $G_l = 30\text{dBi}$. The channel shadow parameters undergo three states: heavy shadowing ($b_k = 0.063,\ m_k = 0.739,\ \Omega_k = 8.97\times10^{-4}$), average shadowing ($b_k = 0.126,\ m_k = 10.1,\ \Omega_k = 0.835$) and light shadowing ($b_k = 0.158,\ m_k = 19.4,\ \Omega_k = 1.29$) [24].

Fig. 2 shows the comparison of ergodic capacity between the NOMA and OMA schemes for different channel shadow parameters with a varying user SNR $\overline{\gamma}_u$, the LEO satellite altitude $h_l = 1400\text{km}$ and the minimal elevation angle $\theta_{\min} = 70^{\text{o}}$, the labels HS/AS/LS denote the channel shadow condition of heavy shadowing, average shadowing and light shadowing, respectively. For all cases, we can observe that the system ergodic capacity of the NOMA scheme are superior to those with the OMA scheme under same channel shadow condition. This observation indicates that the NOMA scheme can not only reuse the frequency resource but also achieve

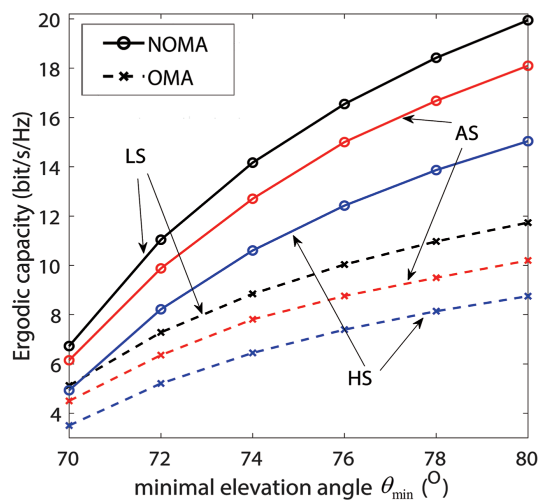

Fig. 4. Ergodic capacity versus minimal elevation angle

higher system capacity. Besides, it can be observed that the capacity gap between the NOMA and OMA scheme degrades when the channel condition gets worse from LS to HS. This is due to the fact that a worse channel condition will decrease the power allocation coefficient α to ensure the capacity requirement of GEO satellite and in turn decrease the capacity gap between the NOMA and OMA schemes.

Fig. 3 depicts the impact of the LEO satellite altitude on the system ergodic capacity with fixed user SNR $\overline{\gamma}_u = 20\text{dB}$ and minimal elevation angle $\theta_{\min} = 70^{\text{o}}$. It can be observed that the ergodic capacities of both NOMA and OMA system degrade as the LEO satellite altitude h_l increases under all three channel shadow conditions. This observation can be explained by the fact that higher LEO satellite altitude corresponds to severe free space loss, thus results in a degradation on the system capacity performance. In addition, we can find that the capacity gaps between the NOMA and OMA scheme degrade as h_l increases, this observation justifies the fact that the NOMA scheme can achieve less capacity gain under smaller channel condition difference.

Fig. 4 shows the system ergodic capacity with different minimal elevation angle $\theta_{\min}$, where $\overline{\gamma}_u = 20\text{dB}$ and $h_l = 1400\text{km}$. As shown in the picture, the ergodic capacity increases with the growth of minimal elevation angle $\theta_{\min}$ because the LEO satellite experience better channel condition with higher elevation angle. In addition, it can be observed that the capacity gaps between the NOMA and OMA schemes increase with larger $\theta_{\min}$. This observation indicates that the transmission link of the LEO satellite operates more effectively in the NOMA scheme, thus improve the spectral efficiency of the considered network.

V. Conclusion

This paper proposes a NOMA enabled a two-layer satellite network in frequency coexistence scenario and analysis the capacity performance of it. Specifically, the ergodic capacity expression is derived and approximated to provide an efficient and intuitive approach for evaluation and demonstration of the NOMA scheme in the proposed scenario. Simulations are provided to confirm the validity of the theoretical analysis and indicate the effect of various parameters on the ergodic capacity performance. Our results reveal the benefit and performance improvement of the considered network, which can be potentially extended into multi-layered satellite scenarios.

Acknowledgment

This work is supported by the Natural Science Foundations of China (No. 61971440, No. 61901502) and the Research project of National University of Defense Technology (NUDT) under grant ZK18-02-11.

References

[1] H. Yao, L. Wang, X. Wang, Z. Lu and Y. Liu, "The Space-Terrestrial Integrated Network: An Overview," *IEEE Commun. Mag.*, vol. 56, no. 9, pp. 178-185, Sept. 2018.

[2] S. K. Sharma, S. Chatzinotas, and B. Ottersten., "In-line Interference Mitigation Techniques for Spectral Coexistence of GEO and NGEO Satellites," *Int. J. Satellite Commun. Netw.*, vol. 34, no. 1, pp. 11-39, 2016.

[3] E. Lagunas, C. G. Tsinos, S. K. Sharma and S. Chatzinotas, "5G Cellular and Fixed Satellite Service Spectrum Coexistence in C-Band," *IEEE Access*, vol. 8, pp. 72078-72094.

[4] K. An, and T. Liang, "Hybrid satellite-terrestrial relay networks with adaptive transmission," *IEEE Trans. Veh. Technol.*, vol. 68, no. 12, pp. 12448-12452, Oct. 2019.

[5] E. Lagunas, L. Lei, S. Chatzinotas and B. Ottersten, "Power and Flow Assignment for 5G Integrated Terrestrial-Satellite Backhaul Networks," 2019 *IEEE Wireless Communications and Networking Conference (WCNC)*, Marrakesh, Morocco, Apr. 2019.

[6] Y. Su, Y. Liu, Y. Zhou, J. Yuan, H. Cao, and J. Shi, "Broadband LEO satellite communications: Architectures and key technologies," *IEEE Wireless Commun.*, vol. 26, no. 2, pp. 55-1, Apr. 2019.

[7] X. Yue, Y. Liu, Y. Yao and et al., "Outage Behaviors of NOMA-Based Satellite Network Over Shadowed-Rician Fading Channels," *IEEE Trans. Veh. Technol.*, vol. 69, no. 6, pp. 6818-6821, June 2020,

[8] Z. Gao, A. Liu and X. Liang, "The Performance Analysis of Downlink NOMA in LEO Satellite Communication System," *IEEE Access*, vol. 8, pp. 93723-93732, 2020.

[9] X. Yan, H. Xiao, C. Wang and K. An, "On the ergodic capacity of NOMA-based cognitive hybrid satellite terrestrial networks," *2017 IEEE/CIC International Conference on Communications in China (ICCC)*, Qingdao, China, 2017.

[10] X Zhang, B Zhang, K. An, and et al, "Outage Performance of NOMA-Based Cognitive Hybrid Satellite-Terrestrial Overlay Networks by Amplify-and-Forward Protocols," *IEEE Access*, vol. 7, pp. 85372-85381, Jun. 2019.

[11] X. Yan, H. Xiao, K. An, G. Zheng and S. Chatzinotas, "Ergodic Capacity of NOMA-Based Uplink Satellite Networks With Randomly Deployed Users," *IEEE Syst. J.*, vol. 14, no. 3, pp. 3343-3350, Sept. 2020.

[12] S. A. Tegos, P. D. Diamantoulakis, J. Xia, L. Fan and G. K. Karagiannidis, "Outage Performance of Uplink NOMA in Land Mobile Satellite Communications," *IEEE Wireless Commun. Lett.*, vol. 9, no. 10, pp. 1710-1714, Oct. 2020.

[13] X. Liu, X. Zhai, W. Lu, and C. Wu, "QoS-guarantee resource allocation for multibeam satellite industrial Internet of Things with NOMA," *IEEE Trans Ind. Informat.*, vol. 17, no. 3, pp. 2052-2061, Mar. 2021.

[14] A. Wang, L. Lei, E. Lagunas, A. I. Prez Neira, S. Chatzinotas and B. Ottersten, "On Fairness Optimization for NOMA-Enabled Multi-Beam Satellite Systems," *2019 IEEE 30th Annual International Symposium on Personal, Indoor and Mobile Radio Communications (PIMRC)*, Istanbul, Turkey, 2019.

[15] X. Zhu, C. Jiang, L. Kuang, N. Ge, and J. Lu, "Non-orthogonal multiple access based integrated terrestrial-satellite networks," *IEEE J. Sel. Areas Commun.*, vol. 35, no. 10, pp. 2253-2267, Oct. 2017.

[16] Z. Lin, M. Lin, J. Wang, T. de Cola and J. Wang, "Joint Beamforming and Power Allocation for Satellite-Terrestrial Integrated Networks With Non-Orthogonal Multiple Access," *IEEE J. Sel. Topics Signal Process.*, vol. 13, no. 3, pp. 657-670, June 2019.

[17] S. Li and C. H. Liu, "An Analytical Model to Predict the Probability Density Function of Elevation Angles for LEO Satellite Systems," *IEEE Communications Letters.*, VOL. 6, NO. 4, pp. 138-140, Apr. 2002.

[18] A. Abdi, W. Lau, M.S. Alouini, and M. Kaveh, "A new simple model for land mobile satellite channels: First- and second-order statistics," *IEEE Trans. Wireless. Commun.*, vol. 2, no. 3, pp. 519-528, May 2003.

[19] I. S. Gradshteyn and I. M. Ryzhik, *Table of Integrals, Series, and Products*, 7th ed. New York, NY, USA: Academic, 2007.

[20] Z. Yang, Z. Ding, P. Fan, and N. Al-Dhahir, "A General Power Allocation Scheme to Guarantee Quality of Service in Downlink and Uplink NOMA Systems," *IEEE Trans. Wireless. Commun.*, vol. 15, no. 11, pp. 7244-7257, Nov. 2016.

[21] M. Abramowitz and I.A. Stegun, *Handbook of Mathematical Functions with Formulas, Graphs, and Mathematical Tables*, 9th ed. New York, NY, USA: Dover, 1972.

[22] V.S. Adamchik and O.I. Marichev, "The algorithm for calculating integrals of hypergeometric type functions and its realization in REDUCE system," in *Proc. ISSAC*, Tokyo, Japan, pp. 212-224, Aug. 1990.

[23] A. M. Mathai and R. K. Saxena, *The H-Function With Applications in Statistics and Other Disciplines*. New York, NY, USA: Wiley, 1978.

[24] K. An, Y. Li, T. Liang, and X. Yan, "On the Performance of Cache-Enabled Hybrid Satellite-Terrestrial Relay Networks," *IEEE Wireless Communications Letters.*, vol. 8, no. 5, pp. 1506-1509, June. 2019.